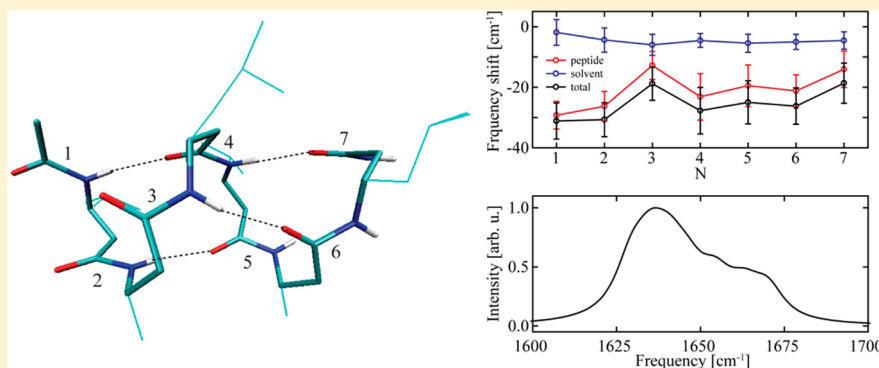


Amide-I Characteristics of Helical  $\beta$ -Peptides by Linear Infrared Measurement and ComputationsJuan Zhao,<sup>†</sup> Jipei Shi,<sup>†,‡</sup> and Jianping Wang<sup>\*,†</sup><sup>†</sup>Beijing National Laboratory for Molecular Sciences, Molecular Reaction Dynamics Laboratory, Institute of Chemistry, Chinese Academy of Sciences, Beijing 100190, P. R. China<sup>‡</sup>University of Chinese Academy of Sciences, Beijing 100049, P. R. China

## S Supporting Information



**ABSTRACT:** In this work, we have examined the amide-I characteristics of three  $\beta$ -peptide oligomers in typical helical conformations (two in 14-helix and one in 12/10-helix), solvated in water, methanol, and chloroform, respectively. Local-mode frequencies and their distributions were computed using a molecular-mechanics force field based frequency map that was constructed on the basis of molecular dynamics simulations. The local-mode frequencies were found to be determined primarily by peptide backbone and side chain, rather by solvent, suggesting their local structural sensitivities. Intermode vibrational couplings computed using a transition dipole scheme were found to be very sensitive to peptide conformation, with their signs and magnitudes varying periodically along the peptide chain. Linear infrared absorption spectra of the three peptides, simulated using a frequency–frequency time-correlation function method, were found to be in fair agreement with experimental results. Normalized potential energy distribution analysis indicated that the amide-I mode can delocalize over a few amide units. However, the IR band structure appears to be more sophisticated in helical  $\beta$ -peptides than in helical  $\alpha$ -peptides.

## I. INTRODUCTION

$\beta$ -peptides, being composed of  $\beta$ -amino acids, are a class of well-known non-natural peptides.<sup>1–4</sup> In the primary structure,  $\beta$ -peptides differ from naturally occurring  $\alpha$ -peptides by one extra backbone carbon methylene unit. The presence of such an extra unit results in three  $\sigma$ -bonds in each amino acid of  $\beta$ -peptides instead of two in the case of  $\alpha$ -peptides, and causes more flexible backbone dihedral angles. The presence of one extra backbone carbon atom also offers more choices to position side chain groups. These are the intrinsic reasons for  $\beta$ -peptides to adopt greater structural flexibility than  $\alpha$ -peptides. Not only can  $\beta$ -peptides form relatively simple structures such as turns and hairpins,<sup>5–8</sup> as similarly seen in  $\alpha$ -peptides, they can also form unique helical conformations that were never seen in  $\alpha$ -peptides. Representative structures of such reported so far are 8-helix,<sup>9</sup> 10-helix,<sup>10,11</sup> 12-helix,<sup>12–15</sup> 14-helix,<sup>16–21</sup> and 12/10-mixed helix,<sup>22,23</sup> which are termed according to the number of atoms participating in intramolecular hydrogen bonds. Thus,  $\beta$ -peptides are believed to be novel structural motifs for studying protein conformational dynamics and

folding problems.<sup>24</sup> Further,  $\beta$ -peptides are also found to exhibit certain biological functions: a transmembrane peptide containing  $\beta^3$ -amino acids has been reported very recently.<sup>25</sup>

It is crucial to understand the structures of  $\beta$ -peptides in order to exploit their useful chemical and/or biological activities.<sup>26</sup> Infrared (IR) spectroscopy has been known for many years as a structural sensitive method. It has been widely used to examine  $\alpha$ -peptide conformations in solution phases. On the basis of the amide-I band (essentially coming from the peptide-bond carbonyl stretch) that appears in the 1600–1700  $\text{cm}^{-1}$  frequency region, an empirical spectrum–structure relationship has been established for  $\alpha$ -peptides.<sup>27</sup> Later, it was recognized that a vibrational excitonic picture can be used to describe a set of interacting amide-I vibrators in various secondary and higher order peptide conformations of  $\alpha$ -peptides.<sup>28–31</sup> The exciton model provides a reasonable

Received: September 26, 2013

Revised: December 12, 2013

Published: December 13, 2013



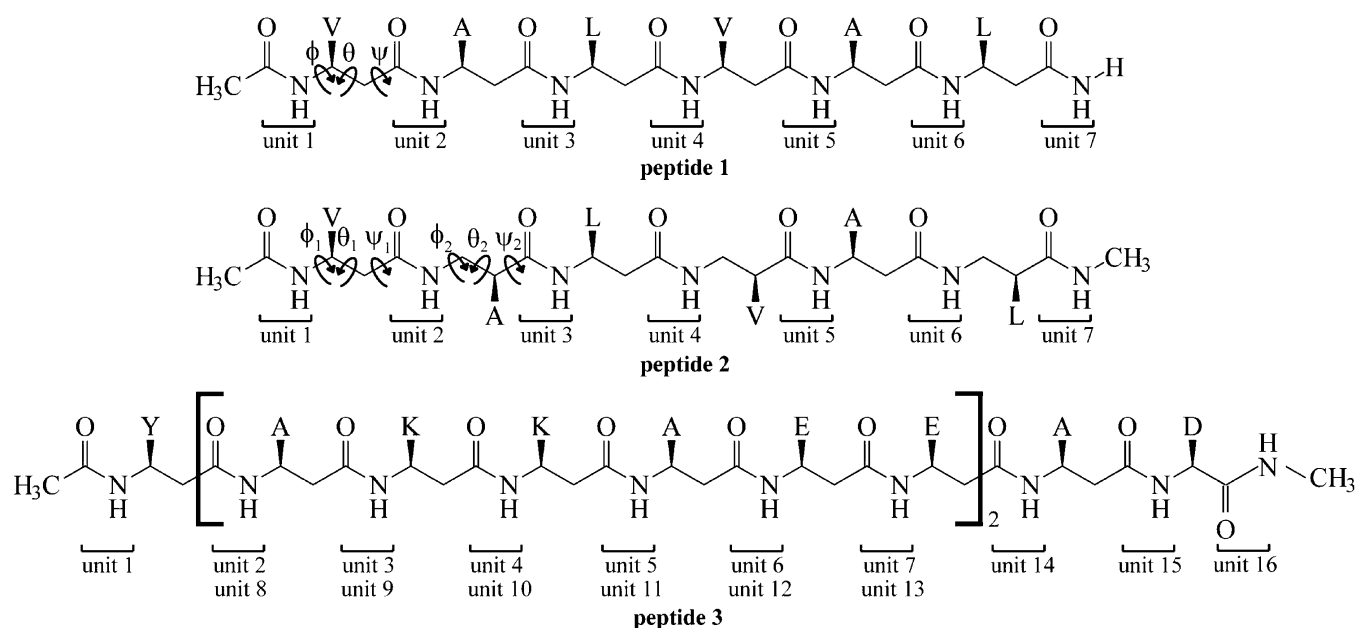


**Figure 1.** Sequence of three helical  $\beta$ -peptides. (a) **Peptide 1:** a 14-helix composed of  $\text{Ac}-(\beta^3\text{-Val}-\beta^3\text{-Ala}-\beta^3\text{-Leu})_2\text{-NH}_2$ . (b) **Peptide 2:** a 12/10-helix composed of heptamer:  $\text{Ac}-\beta^3\text{-Val}-\beta^2\text{-Ala}-\beta^3\text{-Leu}-\beta^2\text{-Val}-\beta^3\text{-Ala}-\beta^2\text{-Leu-NMe}$ . (c) **Peptide 3:** a 14-helix composed of a 16-mer:  $\text{Ac}-\beta^3\text{-Tyr}-(\beta^3\text{-Ala}-\beta^3\text{-Lys}-\beta^3\text{-Lys}-\beta^3\text{-Ala}-\beta^3\text{-Glu}-\beta^3\text{-Glu})_2-\beta^3\text{-Ala-D-Asp-NMe}$ . One letter abbreviations of amino acid residues are given on top of each peptide.

interpretation of the observed spectrum–structure relationship for the amide-I band. In this model, the amide-I modes, which are a subset of  $3N - 6$  normal modes for a given peptide, are treated as a group of coupled anharmonic oscillators. The excitonic Hamiltonian contains zero-order local-mode energies as diagonal elements and interamide-I couplings as off-diagonal elements. After diagonalizing the Hamiltonian, a set of delocalized vibrational states is obtained. Because such an eigen-mode picture only includes a subset of the amide-I modes, it is a simplified version of the normal-mode picture. In the exciton model, the amide-I band of the well-known  $\alpha$ -helix formed by  $\alpha$ -peptide actually contains two closely overlapping bands, namely, the A-mode at the low frequency side and the E-mode at the high frequency side.<sup>32,33</sup> The  $3_{10}$ -helix, even though being seldom seen in reality, has a similar spectral feature.<sup>32,34,35</sup> While in a  $\beta$ -sheet formed by  $\alpha$ -peptide, there are also two peaks in the amide-I region: a low-frequency strong peak that comes from interstrand amide-I oscillators moving in-phase and a high-frequency weak peak that comes from the intrastrand amide-I oscillators moving.<sup>36–38</sup> However, for  $\beta$ -peptides, the spectrum–structure relation and the excitonic nature of the amide-I band have not been fully understood yet.<sup>39</sup>

So far there have been only a few experimental case studies of the vibration spectroscopic signature of  $\beta$ -peptides. Hamm and co-workers examined the structures and structural dynamics of  $\beta$ -peptides in 12/10/12-helical conformations using the narrowband-pump broadband-probe two-dimension infrared (2D IR) technique in the amide-I region.<sup>23</sup> Gai and co-workers examined the folding dynamics of a  $\beta$ -peptide in a 14-helix using temperature-jump aided linear infrared spectroscopy.<sup>24</sup> There are also other spectroscopic investigations of the structures of  $\beta$ -peptide oligomers. For example, Zwier and co-workers investigated the conformational preferences of several model  $\beta$ -peptide oligomers in various intramolecular hydrogen-bonded complexes using two-photon ionization and ultraviolet hole-burning spectroscopies.<sup>26,40–42</sup>

Because there are two carbon atoms separating adjacent amide units rather than one presented in  $\alpha$ -peptides, the vibrational properties of the amide-I mode in  $\beta$ -peptides, including local-mode vibrational frequency, intermode coupling, mode delocalization, pure-mode diagonal anharmonicity, as well as mixed-mode off-diagonal anharmonicity of the amide-I modes in  $\beta$ -peptides, differ from those in  $\alpha$ -peptides. Among these parameters, the first three are important for understanding the linear IR spectroscopy, while all of them are important for understanding the 2D IR spectroscopy of  $\beta$ -peptides.<sup>39</sup> In particular, the amide-I vibrational frequency of  $\beta$ -peptides is of central importance. The eigen-mode picture, as mentioned above, is a representation of a collection of interacting local-mode amide-I oscillators. Here the eigen-mode picture is what we can measure by infrared spectroscopy; however, what behind it is a local-mode picture that contains a set of local-mode frequencies and a set of bilinear intermode couplings. The local-mode frequencies are structurally sensitive, because they are affected by peptide local chemical environment, solvent interactions, as well as intra- and intermolecular hydrogen-bonding interactions. This is well-known for  $\alpha$ -peptides, and is presumably the case for  $\beta$ -peptides. However, due to the greater structural flexibilities of  $\beta$ -peptides, a systematic investigation is necessary. Furthermore, for  $\beta$ -peptides, the side chain can exert position-dependent chemical influences on one hand and steric influences on amide hydrogen bonding on the other hand, both affecting the local-mode frequency of  $\beta$ -peptides.

Computational approaches can be used to predict the amide-I local-mode frequencies, and the obtained results can be used to simulate IR spectra in comparison with experiments, as has been shown in many recent studies of  $\alpha$ -peptide oligomers. There are generally three different approaches. Direct quantum chemistry calculations of peptides in the gas phase at the proper level of theory can be used to predict local-mode frequencies with reasonable accuracy and a set of intermode couplings as a side product.<sup>43–45</sup> However, this method is only suitable for

sizable peptides. On the other hand, the local-mode frequency can also be evaluated at the level of the classical mechanics force field, however, with the shortcoming of being less realistic.<sup>46</sup> Empirical frequency maps have been established for the amide-I local-mode frequencies for  $\alpha$ -peptides by several research groups.<sup>35,47–53</sup> By sampling model peptide and solvent clusters, the electrostatic interaction caused frequency shift from the gas phase to the solution phase can be modeled. The obtained frequency maps can thus be applied to molecular dynamics (MD) trajectories in the frame of classical mechanics, so that a set of time-dependent local-mode frequencies can be computed. The protocol has been used in a number of groups for a number of  $\alpha$ -peptide systems.<sup>34,35,54</sup> Obviously, the advantage of the map approach is the relative easiness to realize; however, its reliability critically relies on how the vibrational chromophore is defined and how the map is constructed. The transferability of the frequency map in different solvents for the  $\alpha$ -peptides has been discussed previously.<sup>51,55</sup>

For  $\beta$ -peptides, however, the evaluation of the amide-I local-mode frequency using the frequency map approach has not been extensively studied yet. Degenerate local-mode frequencies were usually used as initial values in modeling the IR spectra of helical  $\beta$ -peptides.<sup>24,56</sup> In our recent work,<sup>57</sup> by using a  $\beta$ -peptide model compound, *N*-ethylpropionamide ( $\text{CH}_3\text{CH}_2\text{CONHCH}_2\text{CH}_3$ , NEPA), we have examined a molecular-mechanics force field based frequency map (MM-map) in predicting the red-shifted vibrational frequency for the amide-I mode of NEPA in deuterated water ( $\text{D}_2\text{O}$ ). We found that NEPA has the amide-I vibrational characteristics similar to what was seen in the model compound of an isolated  $\alpha$ -peptide, i.e., *N*-methylacetamide (NMA).

In this work, we have chosen three  $\beta$ -peptide oligomers (Figure 1) in helical conformations and compared their linear IR spectra in different solvents for each peptide. **Peptide 1** is a heptamer  $\beta$ -peptide in the 14-helical conformation,<sup>58,59</sup> **peptide 2** is a heptamer  $\beta$ -peptide in the 12/10-helical conformation,<sup>23</sup> while **peptide 3** is a 16-mer  $\beta$ -peptide in a 14-helix with a six-residue repeating structure in the middle.<sup>24</sup> The amide-I local-mode frequencies and their distributions were examined, using our frequency map (the MM-map).<sup>52</sup> MD simulations were performed to sample ultrafast structures of solvated  $\beta$ -peptides and solvent molecules, which were also used to assess the influences of solute and solvent to the frequency shift of the amide-I mode from gas phase to solution phase. Intermode vibrational couplings computed using a transition-dipole coupling (TDC) scheme were compared with those obtained from direct and semiempirical calculation using the PM6 Hamiltonian<sup>60</sup> and the wave function demixing approach.<sup>39,43,61</sup> The structural sensitivity of the coupling was discussed. Linear IR spectra of three  $\beta$ -peptides in the amide-I region were simulated using a frequency–frequency time-correlation function protocol,<sup>62</sup> in comparison with PM6 computational results, and with available experimental results. The IR spectroscopic characteristics and their structural basis for helical  $\beta$ -peptides were discussed with the aid of potential energy distribution function analysis.

## II. MATERIALS AND METHODS

**A. Materials.** *N*-Ethylpropionamide with a purity of 99% was purchased from Sigma-Aldrich. It was lyophilized in deuterated water ( $\text{D}_2\text{O}$ ) three times for H/D exchange for amide group, and then dissolved in  $\text{D}_2\text{O}$  and methanol-*d*

( $\text{CD}_3\text{OD}$ ) with a final concentration of 75 and 85 mM, respectively. The concentration of undeuterated *N*-ethylpropionamide in chloroform ( $\text{CHCl}_3$ ) is 75 mM. **Peptide 1** was synthesized by solid-phase Fmoc chemistry and purified by HPLC to >95% purity. The peptide was dissolved in 0.01 M  $\text{DCl}/\text{D}_2\text{O}/\text{CH}_3\text{CN}$  and lyophilized. The process was repeated three times to achieve a reasonable amount of amide H/D exchange. The lyophilization product was then confirmed by ES-MS. The sample was then dissolved in chloroform-*d* ( $\text{CDCl}_3$ ) with a final concentration of 14.2 mM. This peptide prefers a non-polar solvent environment mainly because of the hydrophobic side chains of both leucine and valine residues.

**B. Infrared Spectroscopy.** The IR spectrum of NEPA was measured using a Nicolet 6700 FTIR spectrometer equipped with a liquid-nitrogen-cooled mercury–cadmium–telluride (MCT) detector. The IR spectra were measured at 23 °C with a spectral resolution of  $1\text{ cm}^{-1}$ , and were averaged by 64 scans. The sample was placed in a homemade demountable IR cell composed of two 2 mm thick  $\text{CaF}_2$  windows with a 50  $\mu\text{m}$  polyester spacer (Du Pont Teijin Films). Dry air was used to purge the FTIR spectrometer and sample chamber during the spectral measurements. The IR spectrum of **peptide 1** in  $\text{CDCl}_3$  was measured with a 19  $\mu\text{m}$  thick spacer under the same experimental conditions. The FTIR spectra of **peptide 2** and **peptide 3** were taken from the literature.<sup>23,24</sup> **Peptide 2** was dissolved in  $\text{CD}_3\text{OD}$ , and **peptide 3** was dissolved in  $\text{D}_2\text{O}$  at concentrations of 15 and 20 mM, respectively, according to the literature.

**C. Molecular Dynamics Simulations.** To sample equilibrium structures on the ultrafast time scale, the MD simulations of NEPA in  $\text{D}_2\text{O}$ ,  $\text{CD}_3\text{OD}$ , and  $\text{CHCl}_3$ , respectively, and **peptide 1** in  $\text{CDCl}_3$ , **peptide 2** in  $\text{CD}_3\text{OD}$ , and **peptide 3** in  $\text{D}_2\text{O}$  were performed using the NAMD simulation program package.<sup>63</sup> The CHARMM force field<sup>64</sup> was used. The main backbone dihedral force field parameters for the three  $\beta$ -peptides were obtained from the parameters optimized by Cui and co-workers.<sup>65</sup> Other parameters were directly taken from the CHARMM force field. All the simulations were carried out in a periodic cubic box. For NEPA, one solute molecule was solvated in 659 TIP3P  $\text{D}_2\text{O}$  molecules,<sup>66</sup> and the side length of the cubic simulation box was set to 28 Å; the side length of NEPA in the  $\text{CD}_3\text{OD}$  solvent cubic box was 30 Å, and there were 464 solvent molecules. The side length of the  $\text{CHCl}_3$  solvent cubic box is 33 Å with 228 solvent molecules. The initial backbone dihedral angles were set according to a recent work:<sup>67</sup>  $[\phi, \theta, \psi] = [-144.1, 59.2, -134.0]$  (in deg) for the 14-helix, and  $[\phi_1, \theta_1, \psi_1; \phi_2, \theta_2, \psi_2] = [-100.6, 61.3, 99.5; 73.5, 68.3, -121.0]$  for the 12/10-helix. For **peptide 1**, the initial side length of the solvent cubic box is 40 Å, containing 499  $\text{CDCl}_3$  molecules. For **peptide 2**, the  $\text{CD}_3\text{OD}$  solvent cubic box is  $40 \times 40 \times 40\text{ Å}^3$  in dimension containing 1043  $\text{CD}_3\text{OD}$  molecules. **Peptide 3** is relatively large in size, so the initial side length of the cubic solvent box was set to 55 Å, containing 5082  $\text{D}_2\text{O}$  molecules. For the MD simulations, the non-bonded cutoff was set to 12 Å, and the particle-mesh Ewald summation<sup>68</sup> was used for long-range electrostatic interactions. The Langevin piston Nosé–Hoover method<sup>69,70</sup> was used for simulation in the isothermal–isobaric ensemble. Each of the MD simulations started from an energy minimization process at 0 K. The MD simulations at room temperature were carried out by a heating process from 0 to 298 K over a 20 ps period. An equilibration process for 1 ns was executed at the desired temperature. The MD simulations



were performed for the NPT ensemble for 10, 6, and 10 ns with a step of 1 fs for **peptide 1**, **peptide 2**, and **peptide 3**, respectively. Atomic coordinates were saved every 2 fs for the first 2 ns simulations and saved every 10 fs for the rest of the simulation times for the three peptides. These MD structures were used to compute the amide-I local-mode frequencies using the MM-map method.<sup>52</sup>

However, for the NPT ensembles, a small volume change occurs during the course of the MD simulations. It is found that the concentration of **peptide 1** fluctuates between 21.3 and 22.8 mM during the 2 ns MD simulations, that of **peptide 2** fluctuates between 22.3 and 23.5 mM during the 4 ns MD simulations, while that of **peptide 3** fluctuates between 11.0 and 11.3 mM during the 10 ns MD simulations. It can be seen that the solute density in each ensemble changes somewhat (less than 7% at most) during the MD simulations. According to the changes of the density or the volume of the three systems, the variation of the local-mode frequencies is estimated to be on the order of 1 cm<sup>-1</sup>. The influence of such a small variation of the local mode frequencies on the simulated IR spectra is automatically taken into account because the MM-map is constructed by random sampling a small subset of structures from a long-time MD trajectory.

**D. Quantum Chemistry and Semi-Empirical Computations.** Structural optimization and harmonic vibration frequency calculation of NEPA in the gas phase were carried out using the density functional theory (DFT) at the level of B3LYP/6-31+G\*. Transition dipole orientations of the amide-I mode were evaluated at the same level of theory. Structural optimization and harmonic vibration-frequency calculations of the three helical  $\beta$ -peptides in the gas phase were carried out using a semiempirical calculation with the PM6 Hamiltonian.<sup>60</sup> Vibrational couplings between pairwise amide-I modes were computed for each system by demixing the wave function of the obtained normal modes, as described previously.<sup>32,71</sup> All calculations were performed using the Gaussian 09 suite of program.<sup>72</sup>

**E. IR Spectral Simulations Using Frequency–Frequency Time-Correlation Function (FTCF).** For the isolated  $\beta$ -peptide monomer, the chromophore of the amide-I oscillator is defined to include not only the deuterated amide unit (COND) but also the two nearby CH<sub>2</sub> groups, as shown in Figure 2. The chromophore is neutral in charge using the

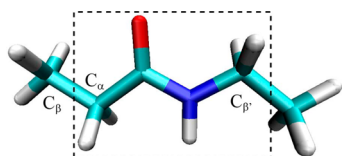


**Figure 2.** NEPA: a model compound with a single amide-I chromophore for  $\beta$ -peptides.

CHARMM force field. Side chains are considered as chemical environments which exert electrostatic forces on the amide chromophore. Several choices of the amide-I chromophore have been tested, and one of which is the amide unit only. It is found that the chromophore shown in Figure 2 works better, judged by local-mode frequencies and their distributions, as well as by the simulated IR spectra described below. Solvent molecules are considered via electrostatic interaction. A similar protocol was used in the case of  $\alpha$ -peptide monomer (NMA).<sup>52</sup>

A molecular-mechanics force-field-based amide-I vibration frequency map, i.e., the MM-map, for  $\alpha$ -peptides was previously constructed.<sup>52,62</sup> Briefly, this is a four-site (C(=O), O(=C), N, and D(=N)) potential model used to account for the red shift of the amide-I frequency of NEPA from the gas phase to the solution phase:

$$\nu = \nu_0 + \sum_i f_i \varphi_i \quad (1)$$

where  $\nu_0$  is a reference value of the NEPA amide-I frequency,  $\varphi_i$  are the electrostatic potentials, and  $f_i$  are their coefficients (MM-map parameters). In eq 1, the electrostatic potentials due to peptide and solvent molecules were taken into account.  $\nu_0$  was set to 1675 cm<sup>-1</sup>, which was the peak position of the instantaneous normal mode (INM) frequency of NEPA obtained using the VIBRAN module of CHARMM<sup>73</sup> for a sample of naked NEPA molecules extracted from MD simulations. Alternatively, one can also use a gas-phase experimental frequency for this value if it were available. 200 MD structures of NEPA in D<sub>2</sub>O were used to model the observed IR frequency of NEPA/D<sub>2</sub>O (1611 cm<sup>-1</sup>, shown in the Supporting Information, Figure S1) using a multivariate least-squares fitting method. In addition, frequency maps were also constructed for the amide-I mode of NEPA solvated in CD<sub>3</sub>OD and CHCl<sub>3</sub> in the same way as NEPA in D<sub>2</sub>O, in order to compute the zero-order vibrational frequency for three solvated  $\beta$ -peptides. This is necessary because  $\beta$ -peptides usually have their preferred solvent environment and even sequence-dependent solubility. Table 1 listed the parameters

**Table 1.** The Frequency Map Parameters (in cm<sup>-1</sup> V<sup>-1</sup>) for the Amide-I Mode of NEPA Solvated in D<sub>2</sub>O, CD<sub>3</sub>OD, and Non-Deuterated NEPA in CHCl<sub>3</sub>

	$f_C$	$f_O$	$f_N$	$f_H$
D <sub>2</sub> O	51.6399	−48.8594	109.3316	−5.9333
CHCl <sub>3</sub>	34.3190	−38.8576	52.8259	−38.2947
CD <sub>3</sub> OD	22.7476	−28.3800	10.6304	2.3264

for the three MM-maps. The linear IR spectrum of each solvated peptide was simulated first using an individual MM-map developed for that specific solute/solvent system. The IR spectra were also simulated using different MM-maps, in order to evaluate the transferability of the maps. It was found that the main features of the IR spectrum of **peptide 1** in CDCl<sub>3</sub> using the MM-map developed in D<sub>2</sub>O or CDCl<sub>3</sub> generally agree with each other, and those of the IR spectrum of **peptide 2** in CD<sub>3</sub>OD using the MM-map developed in D<sub>2</sub>O or CD<sub>3</sub>OD also generally agree with each other (see Figure S2 of the Supporting Information). In this work, only the simulated results using the MM-map developed in D<sub>2</sub>O were given.

By using the MM-map, the local-mode amide-I frequencies of all the amide units in **peptides 1**, **2**, and **3** were obtained by using eq 1. From the first 1 ns MD simulations, 500 000 instantaneous amide-I local-mode frequencies for each amide unit in the three  $\beta$ -peptides were obtained. From the frequency trajectories, the  $i$ th local-mode FFCF (LM-FFCF) can be computed:

$$C_i(t) = \langle \delta\nu_i(t) \delta\nu_i(0) \rangle \quad (2)$$

where  $\delta\nu_i(t) = \nu_i(t) - \langle \nu_i \rangle$  and  $\langle \nu_i \rangle$  is the average local-mode frequency. A two-component exponential function was used to fit the LM-FFCF in each case:

$$C(t) = \sum_{j=1}^2 \Delta_j^2 e^{-t/\tau_j} \quad (3)$$

The results are given in Figure S3 and Table S1 in the Supporting Information.

To simulate the amide-I linear IR spectra of the three  $\beta$ -peptides, a fluctuating Hamiltonian protocol<sup>62</sup> was used. The  $k$ th eigen-mode FFCF (EM-FFCF) was approximated by a linear combination of the LM-FFCFs:<sup>54,62</sup>

$$\begin{aligned} C_k(t) &= \langle \delta\nu_k(t) \delta\nu_k(0) \rangle \\ &= \sum_i V_{ik}^{-4} \langle \delta\nu_i(t) \delta\nu_i(0) \rangle \end{aligned} \quad (4)$$

Here  $V$  is the eigenvector obtained from diagonalizing the fluctuating local-mode Hamiltonians composed of local-mode frequencies as diagonal elements and the TDC values<sup>32,74</sup> as off-diagonal elements. 500 000 MD structures were used to construct the local-mode Hamiltonians. The computed EM-FFCFs for the three  $\beta$ -peptides obtained at room temperature were then fitted biexponentially. The results are given in Figure S4 and Table S2 in the Supporting Information.

The line shape function  $g(t)$  for the  $k$ th eigen-mode can be obtained with the aid of the cumulant expansion method:<sup>75–77</sup>

$$g_k(t) = \int_0^t dt_1 \int_0^{t_1} \langle \delta\nu_k(t_2) \delta\nu_k(0) \rangle dt_2 \quad (5)$$

The linear IR absorption spectrum of the  $i$ th eigen-mode can be computed

$$I_k(\nu) = \int_{-\infty}^{+\infty} e^{-i(\nu_k - \langle \nu_k \rangle)t - g_k(t) - t/2T_1} dt \quad (6)$$

Here  $T_1$  is the lifetime of the first vibrational excited state of the amide-I mode of peptide, which was set to 0.5 ps, which is typical for the amide-I mode in  $\alpha$ -peptides.<sup>78</sup> The overall amide-I band of each  $\beta$ -peptide was computed by  $I(\nu) = \sum_k |\mu_k|^2 I_k(\nu)$ , where  $|\mu_k|^2$  is the transition dipole strength of the  $k$ th eigen-mode. Note that the structures of **peptide 2** and **peptide 3** used in our simulations are different in terminal groups from those used in experiments,<sup>23,24</sup> to avoid additional force-field parametrizations. In addition, the capping amide units in **peptide 2** and **peptide 3** are not considered in our spectral simulation. Structural details are given in Figure S5 of the Supporting Information. These variations do not change the main structure of the two helices.

### III. RESULTS AND DISCUSSION

**A. IR Spectra of Three Peptides.** Figure 3 shows experimental linear IR spectra of **peptide 1** in  $\text{CDCl}_3$ , **peptide 2** in  $\text{CD}_3\text{OD}$ , and **peptide 3** in  $\text{D}_2\text{O}$ , respectively, in the spectral region of 1520–1730  $\text{cm}^{-1}$ . **Peptide 1** mainly exhibits a broad absorption band peaked at 1641  $\text{cm}^{-1}$ , with a clear high-frequency shoulder component shown at ca. 1665  $\text{cm}^{-1}$ . The total full width at half-maximum (fwhm) is found to be 56  $\text{cm}^{-1}$ . Curve fitting using Gaussian functions can yield seven components, with peak positions at 1598.9, 1612.6, 1626.4, 1638.6, 1650.7, 1665.1, and 1678.8  $\text{cm}^{-1}$ , respectively (fitted component not shown). Note that the broad band between 1520 and 1600  $\text{cm}^{-1}$  is due to the residual amide-II mode absorption (N–H in-plane bending plus C–N stretching). **Peptide 2** exhibits a two-band absorption feature, with two main components peaked at 1635 and 1680  $\text{cm}^{-1}$ , and total

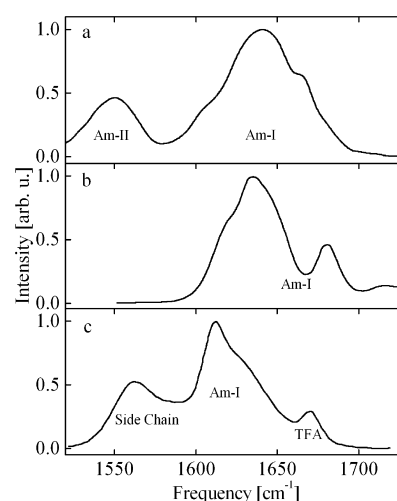


**Figure 3.** Experimental linear IR spectra of **peptide 1** in  $\text{CDCl}_3$  (a), **peptide 2** in  $\text{CD}_3\text{OD}$  (b), and **peptide 3** in  $\text{D}_2\text{O}$  (c). The latter two spectra were taken from the literature<sup>23,24</sup> with permission. Only the spectral range of the amide-I and -II modes is shown.

fwhm found to be 42  $\text{cm}^{-1}$  for the low-frequency component. The curve fitting with Lorentzian function shows four subcomponents peaked at 1618, 1634, 1647, and 1681  $\text{cm}^{-1}$ , respectively.<sup>23</sup> **Peptide 3** shows a strong absorption at 1612  $\text{cm}^{-1}$  (fwhm = 39  $\text{cm}^{-1}$ ); three main components were obtained by curving fitting:<sup>24</sup> 1612, 1624, and 1650  $\text{cm}^{-1}$ . Here the broad band between 1540 and 1600  $\text{cm}^{-1}$  is due to the deprotonated  $\beta^3$ -hGlu and D-Asp side chains, while the peak at 1673  $\text{cm}^{-1}$  is due to trifluoroacetic acid during peptide synthesis.<sup>24</sup> Note that there are seven amide units in **peptide 1**, five in **peptide 2**, and 14 in **peptide 3**, which cannot be directly reflected by the apparent spectral fittings given above, due to the normal-mode nature of the amide-I band.

The amide-I profile for the 14-helix is found to be both peptide sequence dependent and solvent dependent (Figure 3a and c). In  $\text{D}_2\text{O}$ , there are solvent–peptide hydrogen-bonding interactions, which cause more red shift in the main peak position (Figure 3c). The 14-helix and 12/10-helix have different spectral features. For the 14-helical structure, frequency separations between the main peak and its low- and high-frequency components are limited, while for the 12/10-helix, there are two apparent peaks with frequency separation (ca. 45  $\text{cm}^{-1}$ ) much larger than the typical homogeneous bandwidth of the amide-I mode (tens of  $\text{cm}^{-1}$ ). The difference of the amide-I profile between the 14- and 12/10-helices can be mainly attributed to their different intramolecular hydrogen-bonding structures (see below). Further, it is interesting to compare the signature of  $\beta$ -peptide in 14-helix and  $\alpha$ -peptide in  $\alpha$ -helix in  $\text{D}_2\text{O}$ . For the 14-helix, there is a strong absorption at 1612  $\text{cm}^{-1}$  with an asymmetric line shape, while for the  $\alpha$ -helix, the amide-I band is typically peaked at ca. 1650  $\text{cm}^{-1}$  with a Gaussian-like line shape, as shown in a previous work.<sup>79</sup> These results indicate that the helical  $\beta$ -peptide has quite a sophisticated amide-I band structure, which is also quite different from the case in the helical  $\alpha$ -peptide.

**B. Amide-I Local-Mode Frequencies of the Three  $\beta$ -Peptides.** In order to understand the observed linear IR spectra of the helical  $\beta$ -peptides, we shall examine their local mode frequencies using the MM-map described above.

However, before we begin, we first examine the solvated structures of the three peptides.

Figure 4 depicts typical three-dimensional (3D) structures of the three  $\beta$ -peptides. These are the initial structures for the MD

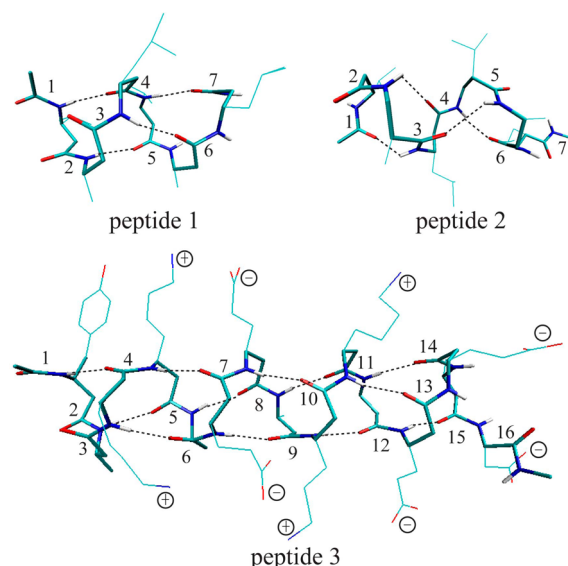


**Figure 4.** Typical three-dimensional (3D) structures of the three helical  $\beta$ -peptides. Charges on the side chains are also marked in peptide 3.

simulations. The dihedral angles are set according to a recent work,<sup>67</sup> in which average dihedral angles for the 14-helix are predicted to be  $[\phi, \theta, \psi] = [-144.1, 59.2, -134.0]$  (in deg), and those for the 12/10-helix are predicted to be  $[\phi_1, \theta_1, \psi_1; \phi_2, \theta_2, \psi_2] = [-100.6, 61.3, 99.5; 73.5, 68.3, -121.0]$ . There are two sets of dihedral angles for the 12/10-helix. The obtained results are in general agreement with a previous report.<sup>80</sup> The analysis of backbone dihedral angles and their distributions are carried out for the MD simulations of the three peptides. Average dihedral angles and standard deviations extracted from all the MD trajectories are listed in Table 2, and the populations of these angles for the first 1 ns MD trajectories are plot in Figure S6 of the Supporting Information. Narrow distributions are found for most dihedral angles. Thus, during the 1 ns MD simulations, the three peptides maintain their original secondary structure, except the C-terminal region of **peptide 1** and **peptide 2**: the last pair of the dihedral angles shows certain variations. Because of different spatial geometries, these  $\beta$ -peptides can have inhomogeneous backbone solvation, meaning solvent molecules can have different distributions around the amide units located at different sections of the peptide chain. This differs from the case of  $\alpha$ -peptides in the  $\alpha$ -helical conformation, where a homogeneous backbone solvation can be found.

We now compute the local-mode frequencies, and the results are given in Figure 5. We also examine the influence from peptide (backbone and side chain) and solvent interactions separately. Figure 5a–c shows the average frequency shift (from  $1675\text{ cm}^{-1}$ ) of the amide-I local modes for the three  $\beta$ -peptides. The total frequency shifts and shifts due to peptide and solvent are shown separately. It is seen that solvent induced frequency shifts are generally smaller than those induced by peptides. For **peptide 1** solvated in  $\text{CDCl}_3$ , the frequency shift is dominated by the contribution from the peptide backbone and side chains.

**Table 2.** Average Backbone Dihedral Angles (in deg) Obtained from the 2 ns MD Trajectory for Peptide 1, 4 ns MD Trajectory for Peptide 2, and 10 ns MD Trajectory for Peptide 3<sup>a</sup>

peptide 1			
	$\phi$	$\theta$	$\psi$
1	−155.7 (9.9)	65.3 (7.7)	−123.8 (13.8)
2	−145.9 (12.7)	58.5 (8.6)	−132.1 (13.2)
3	−139.5 (13.6)	61.2 (7.8)	−142.9 (11.4)
4	−127.5 (10.3)	55.6 (8.1)	−124.6 (13.4)
5	−145.1 (14.4)	58.9 (8.5)	−135.5 (12.4)
6	−125.7 (14.3)	70.1 (9.5)	58.9 (20.3)
peptide 2			
	$\phi$	$\theta$	$\psi$
1	−113.9 (13.4)	61.8 (8.8)	78.7 (12.4)
2	97.9 (15.3)	69.5 (8.1)	−97.3 (10.8)
3	−109.3 (10.7)	59.9 (7.6)	81.9 (11.8)
4	96.2 (14.2)	70.2 (8.7)	−100.7 (11.4)
5	−110.0 (11.9)	66.2 (8.2)	84.3 (12.1)
6	68.4 (12.8)	72.7 (9.2)	−108.0 (12.6)
peptide 3			
	$\phi$	$\theta$	$\psi$
1	−136.8 (20.1)	68.3 (9.4)	−103.1 (22.3)
2	−133.5 (18.9)	64.3 (9.1)	−110.1 (14.8)
3	−138.9 (15.5)	61.1 (9.0)	−124.6 (14.0)
4	−142.9 (14.0)	62.2 (8.3)	−124.6 (13.2)
5	−141.9 (13.4)	60.1 (8.6)	−127.1 (13.7)
6	−140.8 (13.5)	62.3 (8.3)	−128.3 (13.2)
7	−137.0 (13.7)	59.0 (8.8)	−126.4 (13.4)
8	−141.2 (13.4)	60.5 (8.5)	−126.0 (12.9)
9	−138.8 (13.5)	59.0 (8.3)	−127.0 (13.2)
10	−139.4 (13.4)	59.4 (8.5)	−125.3 (13.6)
11	−140.9 (13.7)	61.7 (8.7)	−107.3 (13.0)
12	−140.4 (13.7)	62.8 (8.2)	−128.1 (13.8)
13	−138.6 (14.0)	62.0 (8.4)	−118.5 (15.8)
14	−140.1 (15.3)	61.9 (9.1)	−112.6 (14.7)

<sup>a</sup>The standard deviations of the dihedral angles are in parentheses.

Solvent influence is only one-third on average of that from the peptide structures. Further, since **peptide 1** is formed by all the  $\beta^{\text{D}}$ -amide acid, differences of the red-shift for the first through seventh amide-I local modes caused by the side chain are expected to be small. Thus the main factor is the backbone. However, the total shifts for the third and seventh amide-I modes are less than the remainders. This is because the third amide unit has a rich chemical environment, while the seventh amide unit is located on the C-terminal end.

As shown in Figure 5b, for **peptide 2** solvated in  $\text{CD}_3\text{OD}$ , the frequency shifts caused by peptide are larger than those caused by solvent except for unit 2, and the trend of the total frequency shift is similar to that caused by the peptide. The solvent effects on unit 2 and unit 6 are larger (more red shift) than that on the remainder units, which may be due to better local solvation around the two terminal amide units. In addition, because the dihedral angles for the adjacent amide acid are different in the 12/10-helix, the frequency shifts for these units caused by peptide itself are different: the frequency shifts for unit 2, unit 4, and unit 6 are smaller than those for unit 3 and unit 5. From the 3D backbone structures of **peptide 2** (see Figure 4), we can see these five amide units form different hydrogen bonds: the hydrogen bond for unit 2 and



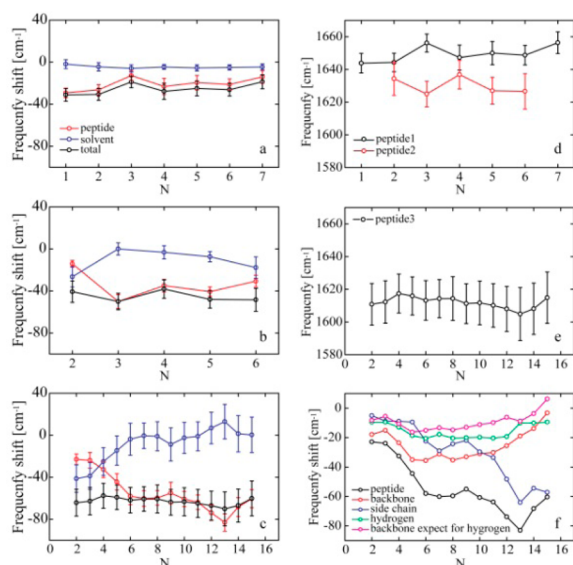


**Figure 5.** Average frequency shift of the amide-I mode and contributions due to peptide and solvent for **peptide 1** (a), **peptide 2** (b), and **peptide 3** (c); average local-mode frequency for **peptides 1** and **2** (d) and **peptide 3** (e); and frequency shift due to the different parts of peptide for **peptide 3** (f). Error bars indicate standard deviations.

unit 5 is at the N—H site, while it is at the C=O site for unit 6. For units 3 and 4, both C=O and N—H groups form a hydrogen bond, so the frequency shifts caused by hydrogen bonding interactions for units 2 and 5 are the smallest (ca. 8 cm⁻¹), and those for unit 3 and unit 4 are the largest (ca. 19 cm⁻¹). Considering all the reasons for the frequency shift, the frequency shift for unit 2 due to peptide is the smallest.

For **peptide 3** solvated in D<sub>2</sub>O, the frequency shift due to solvent is also smaller than that due to the peptide. It is noted that overall the frequency shift is larger than those of **peptide 1** and **peptide 2**, which is mainly due to charged side chain groups, as shown in Figure 4. A detailed component analysis for **peptide 3** is further carried out, and the result is given in Figure 5f.

These results suggest a significant mode dependence in the total shifts and their contributions from peptide and solvent, as well as the final values of the local-mode frequencies shown in Figure 5d,e, suggesting a complicated intramolecular chemical environment of  $\beta$ -peptides that are also inhomogeneously solvated. Nevertheless, the amide-I frequency shift is found to be mainly caused by peptide backbone and side chains in  $\beta$ -peptides in three typical solvents. This implies that the amide-I mode in  $\beta$ -peptides is of more structural sensitivity than in  $\alpha$ -peptides. As shown very recently by Ge and her co-workers,<sup>35</sup> for an artificial  $\alpha$ -peptide in a 3<sub>10</sub>-helix, the amide-I frequency shift due to solvent (CDCl<sub>3</sub>) is either comparable to or larger than that due to peptide, when evaluated using several frequency maps. Furthermore, Figure 5 shows that, even though the solvent-induced frequency shift is not dominant, overall D<sub>2</sub>O caused the largest frequency shift, while CDCl<sub>3</sub> caused the smallest shift. Thus, the nature of solvent is reflected by the frequency shift. This is expected because the frequency maps are based on electrostatic potential and CDCl<sub>3</sub> is much less polar than D<sub>2</sub>O. The inhomogeneous solvation and local structural influences on local-mode frequency distributions have been known for  $\alpha$ -peptides, for example, in the case of

tryptophan zipper 2.<sup>53,81–83</sup> In an early study,<sup>56</sup> the local-mode frequency fluctuations of a  $\beta$ -peptide heptamer in a 14-helix were estimated by taking into account hydrogen-bonding interaction only, whereas, in a recent study of a 15-residue 14-helical  $\beta$ -peptide,<sup>24</sup> a single value of the diagonal element was assumed. Our analysis here suggests that the structural and solvation aspects of the local-mode frequency should be taken into account in modeling the amide-I properties of the  $\beta$ -peptides.

**C. Intermode Couplings.** Pair-wise vibrational coupling of the amide-I modes, on the other hand, is one of the key factors for the amide-I absorption band to exhibit 3D structural sensitivity to the peptides and proteins. This is because the magnitude and sign of coupling depend on the relative orientation and distance of the interacting transition dipoles in dipole approximation,<sup>28</sup> or the interacting amide units in charge flux<sup>32,74</sup> or charge density approximation.<sup>31,84</sup> As shown in our recent quantum chemistry computations, the interamide-I couplings in  $\beta$ -peptides are generally weaker than those in  $\alpha$ -peptides; however, both exhibit sensitivities to the backbone dihedral angles.<sup>39</sup>

Figure 6 shows the contour plots of average bilinear transition dipole coupling constants of the amide-I modes of

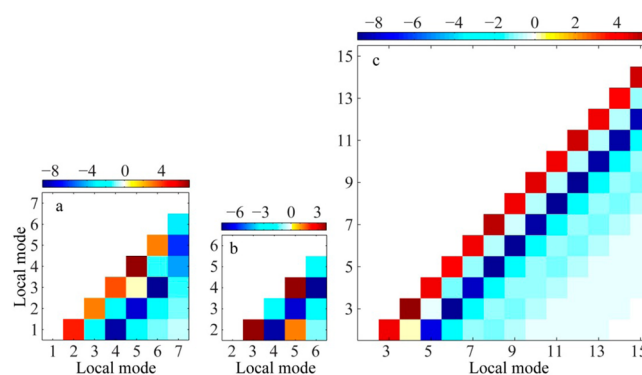


**Figure 6.** Average TDC values of the amide-I modes of **peptide 1** (a), **peptide 2** (b), and **peptide 3** (c).

**peptides 1, 2, and 3.** To compute the TDC, we first optimize the geometric properties of the amide-I transition dipole in an isolated peptide unit, i.e., NEPA. With a followed Hessian calculation, the magnitude of the transition dipole moment is found to be  $|\Delta\mu| = 0.247$  D, with an orientation angle found to be  $\theta = 19.7^\circ$  with respect to the C=O bond direction (pointing from C to O). This result is quite similar to what was seen in the mono amide unit of  $\alpha$ -peptide in magnitude but slightly different in orientation (NMA, with  $|\Delta\mu| = 0.268$  D and  $\theta = 13.4^\circ$ ).<sup>44</sup> The interamide-I coupling between the  $i$ th and  $j$ th units, denoted by  $\beta_{ij}$ , ranges from ca.  $-8.8$  to  $+6.9$  cm⁻¹ in the TDC approximation for the three peptides. Our recent quantum chemistry computations revealed that, in  $\beta$ -HADP, a model  $\beta$ -dipeptide, interamide-I coupling varies from  $-5.7$  to  $+5.6$  cm⁻¹.<sup>39</sup> These results are in reasonable agreement. These couplings are generally smaller than those of the glycine  $\alpha$ -dipeptide, which range from  $-13.2$  to  $+17.8$  cm⁻¹ within the transition dipole approximation.<sup>43</sup> The generally smaller couplings in  $\beta$ -peptides are mainly caused by the additional methylene in the backbone of the  $\beta$ -peptides, which increases the distance between pairwise amide units, regardless of their orientations.

The sign and magnitude of the TDC are sequence dependent. Strong interaction occurs between pairs of hydrogen-bonded amide units. The 14-helix is stabilized by hydrogen bonding between the amide NH group at position  $i$  and the amide carbonyl group at position  $i + 3$  (see Figure 4a and c), so the strongest negative coupling occurs between the  $i$ th and  $(i + 3)$ th amide units, meaning  $\beta_{i,i+3}$  is the strongest negative coupling. The nearest neighbors have the strongest positive coupling, i.e.,  $\beta_{i,i+1}$  is the strongest positive coupling. This can be clearly seen in the color pattern shown in Figure 6a and c. Also, because the 14-helix has a three-residue repeating period, as far as hydrogen bonding interaction is concerned, the coupling is similar every three amide groups, for example, between unit 2 and unit 3, that between unit 5 and unit 6, between unit 8 and unit 9, and so on. These nearest neighboring couplings are positive in sign. In the 12/10-helical structure, the 12-membered hydrogen bonding occurs between amide unit  $i$  and unit  $i + 2$ , while the 10-membered hydrogen bonding is formed between amide unit  $i + 1$  and amide unit  $i + 3$  (see Figure 4b). Thus, both the 12- and 10-membered rings have hydrogen bonding linkage between every two amide units, so the couplings are similar between every two amides. For example, the coupling between unit 2 and unit 3 is about the same as that between unit 4 and unit 5, and the coupling between unit 3 and unit 4 is similar to that between unit 5 and unit 6. These general rules of couplings for the 12/10-helix structure can also be seen from the color pattern shown in Figure 6b. To conclude, the diversity of the vibrational couplings in  $\beta$ -peptides will cause delocalization of the amide-I modes in an apparently more complicated way than usually seen in the case of typical conformations in the  $\alpha$ -peptides (e.g.,  $\alpha$ -helix and  $\beta$ -sheet). Nevertheless, these simple rules of significant couplings in the 14-helical and the 12/10-helical conformations are useful in modeling and understanding the essential signature of their IR spectra of the  $\beta$ -peptides.

Further, Figure 7 compares vibrational couplings obtained from the TDC scheme and from the wave function demixing scheme on the level of the PM6 method. The couplings are

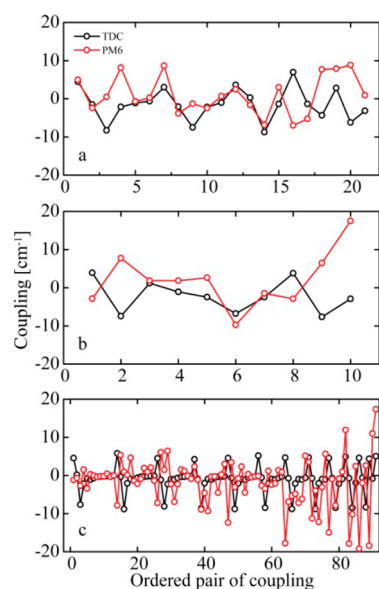


**Figure 7.** Vibrational couplings from the TDC approach (black) and the wave function demixing approach (red) using the PM6 method for the amide-I modes of **peptide 1** (a), **peptide 2** (b), and **peptide 3** (c).

taken from Table S3 of the Supporting Information, and are arranged in the order of row (from top to bottom) and of column (from left to right). It shows that the PM6 couplings generally follow the TDC values; however, exceptions do exist. For example, for **peptide 2**,  $\beta_{56} = -2.9 \text{ cm}^{-1}$  by the TDC method but  $17.5 \text{ cm}^{-1}$  by the PM6 method. A direct comparison of these coupling constants is given in Table S3 (Supporting Information).

**D. Linear Infrared Spectral Simulations.** We first compute local-mode frequency–frequency time-correlation functions (LM-FFCFs) of each helical  $\beta$ -peptide. These data are used to compute eigen-mode FFCFs using eq 4, which are assumed to be linear combinations of the LM-FFCFs. These results are shown in Figures S3 and S4 (Supporting Information), and their double exponential fitting parameters are listed in Tables S1 and S2 (Supporting Information). The LM-FFCFs and EM-FFCFs show a fast component with a sub-100 fs time constant and a slow component with a few ps time constant, clearly indicating a separation of time regime between the two components. The fast component falls into the motional narrowing limit, while the slow component is close to a static inhomogeneous limit. This is the reason that the cumulant expansion method<sup>75–77</sup> can be used in our modeling. However, because the frequency–frequency time-correlation approach is used, both the homogeneous and inhomogeneous line broadenings are taken into account.

Simulated linear IR absorption spectra of three  $\beta$ -peptides are shown in Figure 8. By comparing with the results in Figure 3,

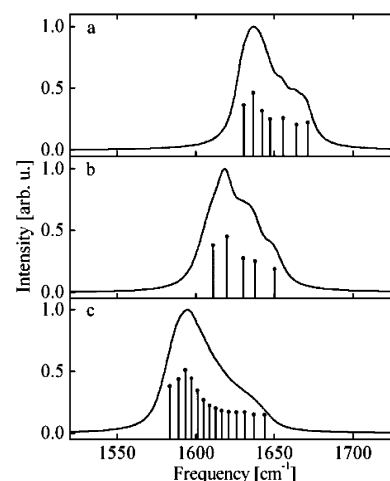


**Figure 8.** Simulated IR spectra of **peptide 1** in  $\text{CDCl}_3$  (a), **peptide 2** in  $\text{CD}_3\text{OD}$  (b), and **peptide 3** in  $\text{D}_2\text{O}$  (c), with sticks showing eigen-mode frequency positions and transition intensities.

one sees that the simulations show some basic band structures of experimentally observed IR spectra. The rough agreement mainly lies in the relative order of the peak positions and overall band shapes. However, there are some differences between simulation and experiments.

For **peptide 1**, the simulated IR spectrum shown in Figure 8a is peaked at  $1636.5 \text{ cm}^{-1}$ , which is ca.  $4 \text{ cm}^{-1}$  blue-shifted from the experimental peak position. Further, there is a pronounced high-frequency shoulder. The overall fwhm is predicted to be  $34 \text{ cm}^{-1}$ , which is somewhat narrower than the experimental result.

For **peptide 2**, the simulated IR spectrum shown in Figure 8b is peaked at  $1618.5 \text{ cm}^{-1}$ , which is  $16.7 \text{ cm}^{-1}$  lower than the



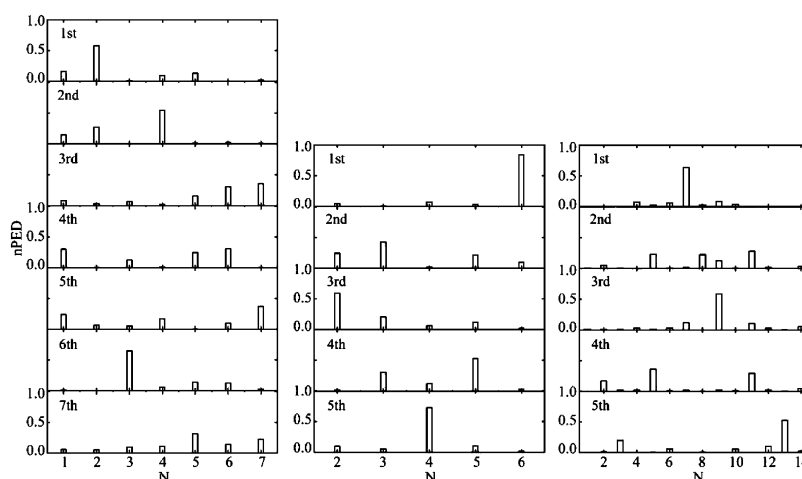


**Figure 9.** Contributions of each local mode to the eigen-modes for **peptide 1** (left) and **peptide 2** (middle) and to the five strongest eigen-modes of **peptide 3** (right) in terms of the normalized PED. Eigen-mode labeling starts from the low-frequency side, as shown by sticks in Figure 8.

experimental peak position. It shows both a low-frequency and high-frequency shoulder, with a total fwhm predicted to be  $36\text{ cm}^{-1}$ , which is similar to the experimental results. On the other hand, the relatively sharp spectral feature agrees fairly with experimental results. The capping groups of **peptide 2** (shown in Figure S5, Supporting Information) used in our simulation are different from those in Hamm's work;<sup>23</sup> their first and seventh amide units are not included in our simulation. This is the reason why a high-frequency weak component is missing in Figure 8b as compared with the experimental result shown in Figure 3b. These terminal and non-hydrogen-bonded amide groups were known to contribute to the high-frequency component ( $1681\text{ cm}^{-1}$  by experimental observation).<sup>23</sup>

For **peptide 3**, the simulated IR spectrum (Figure 8c) shows a main peak at  $1595\text{ cm}^{-1}$ , which is  $17.8\text{ cm}^{-1}$  blue-shifted from the experimental peak position. However, a total fwhm of  $38\text{ cm}^{-1}$  is predicted by simulation, which agrees fairly with the IR experiment. In this case, unlike the previous study,<sup>24</sup> by obtaining a set of non-degenerate local-mode frequencies, our simulation reproduces the high-frequency components with reasonable intensities. Further, because the aqueous solvent environment has been considered in constructing the MM-map in our modeling, the main peak for **peptide 3** is the most red-positioned among the three cases. This prediction is also in agreement with experiments.

In addition, to better compare the simulations with experiments, we add additional frequency shift to the peak positions of the simulated IR spectra. The results are given in Figure S7 (Supporting Information). Again, as can be seen, the agreement between simulations and experiments is fairly reasonable. However, the differences between the simulations and experiments suggest that our modeling protocols require further refinement, at least in three aspects: models for the local-mode frequencies, longer MD simulations for more reasonable structural samplings, and models for the vibrational couplings, in particular those between the nearest neighbors as in the case of  $\alpha$ -peptides.<sup>32,85,86</sup>

Also, the calculated IR spectra of the three  $\beta$ -peptides in the gas phase using the semiempirical PM6 method are shown in Figure S7 (Supporting Information) with slightly different frequency scaling factors for better comparison. The calculations are carried out based on a single structure in each case.

Next, to evaluate the structural basis of the amide-I band profiles of three  $\beta$ -peptides, we examine the strength of the potential energy distribution (PED), i.e., the normalized PED (nPED), which contains a contribution coefficient of each local-mode oscillator to a given eigen-mode. We find the normalized PED is a better presentation of mode delocalization degree than PED itself.<sup>87</sup> The frequencies and strengths of eigen-mode oscillators are illustrated as sticks in Figure 8. Only five low transition energy modes (including the strongest transition) are considered in **peptide 3**. The results of the PED analysis are given in Figure 9. Significant mode delocalization is seen in most cases, suggesting the eigen-mode nature of the amide-I modes. However, in certain cases, one can see highly localized modes. For example, the nPED analysis demonstrates that the amide-I component with the sixth eigen-mode in **peptide 1** is mainly due to the third amide unit, which is clearly free of hydrogen-bonding interaction (Figure 4). In **peptide 2**, the amide-I component with the first lowest-energy eigen-mode is mainly due to the sixth amide unit, even though it is hydrogen-bonded to the fourth amide unit (Figure 4). In **peptide 3**, the lowest transition energy eigen-mode is moderately localized on the seventh amide unit, which sits in the middle of the peptide chain and is hydrogen-bonded with its C=O and N—H groups both. These nPED results can be used to reveal the structural basis of each eigen-mode. It can be used to link the underlying subcomponents in the IR absorption band in the eigen-mode picture to the individual amide-I chromophores in the local-mode picture. The results also show the nPED patterns of the eigen-modes starting from the low-frequency side in the two 14-helices (**peptide 1** and **peptide 3**) do not agree with each other; this is particularly so for the components located near the main peak position. This suggests that the structural basis of the peak transition of the 14-helix is chain length dependent. In addition, for the 14-helix, mode delocalization involves a few amide units. To summarize this section, the nPED analysis suggests that the amide-I mode in  $\beta$ -peptides is delocalized over a few amide units, which is in fact very similar to the case of  $\alpha$ -peptides that has been well studied.<sup>31,44,74</sup>

#### IV. CONCLUDING REMARKS

In this manuscript, peptide backbone structure and structural distributions, amide-I local-mode and eigen-mode frequencies,

and experimental and computed IR absorption spectra of three typical helical  $\beta$ -peptides each solvated in a different solvent (chloroform, methanol, and water, respectively) were examined. The solution-phase local-mode frequencies and their distributions were evaluated using the empirical frequency map (MM-map), which was developed on the basis of the molecular-mechanics force field, using an optimized choice of amide-I chromophore on NEPA. The MM-maps in different solvents were constructed with the aid of MD simulations using explicit solvent models. The MD simulations were also utilized to sample structures of solvated  $\beta$ -peptides and solvent molecules. The MM-map was used to assess the factors that cause amide-I vibrational frequency shift from the gas phase to the solution phase. The factors include the peptide main chain, side chain, as well as solvent molecules. Linear infrared spectra of the amide-I modes of the three peptides were then simulated using a frequency–frequency time-correlation function protocol, and the results were compared with available FTIR experiments.

The local-mode frequencies are found to be both structurally sensitive and solvent sensitive, suggesting a complicated chemical environment and inhomogeneous solvation of  $\beta$ -peptides. The hydrogen bonding interactions and type of side chain groups (neutral and charged) all affect the frequency shift of the amide-I local mode. Even though the solvent-induced frequency shift is not dominant, overall the nature of solvent can be reflected by the frequency shift. One of the significant consequences of such results is that the amide-I mode is perhaps more structurally sensitive in  $\beta$ -peptides than in  $\alpha$ -peptides. Thus, the structural and solvation aspects of the local-mode frequency should be taken into account in modeling the amide-I properties of the  $\beta$ -peptides.

Intermode vibrational couplings for the amide-I modes in the 14-helical and 12/10-helical conformations computed using a transition-dipole scheme were found to obey certain rules: the sign and magnitude varied periodically along the peptide chain, thus exhibiting local structural sensitivity. In particular, the simple rules of significant couplings would be useful in modeling and understanding the essential signature of their IR spectra of the  $\beta$ -peptides. However, compared with the case in  $\alpha$ -helices, the couplings were generally smaller in  $\beta$ -peptides, which were mainly due to the additional methylene in the backbone of the  $\beta$ -peptides that increased the distance between pairwise amide units.

The characteristics of the simulated IR spectra of the amide-I mode for the three  $\beta$ -peptides were generally consistent with the experimental spectra, suggesting the usefulness of the map approach to mapping the local-mode frequencies. The spectrum–structure relationship of helical  $\beta$ -peptides was further discussed on the basis of the analysis of the normalized potential energy distributions, which is a better measure of the delocalization degree of the amide-I eigen-modes. The results suggested that the amide-I mode delocalizes over a few amide units in all cases.

However, it has to be pointed out that, because of the structural diversity of  $\beta$ -peptides, the MM-map approach for local-mode amide-I frequencies needs further refinement, in order to better reproduce the simulated main peak position as well as the total line width. The model also needs to be tested on other  $\beta$ -peptide conformations. This will be done in a future work. The importance of the local-mode frequencies to the simulated IR spectra has also been known in  $\alpha$ -peptides.<sup>53</sup> In

addition, proper solvent models and improved force fields are also needed to be considered in future work.

In summary, the computational results in this work allow us to gain a better understanding of the structural basis of the vibrational properties of the amide-I modes in helical  $\beta$ -peptides. We have tested and established a protocol for simulating the amide-I modes of  $\beta$ -peptides. Simulation and experimental studies of 2D IR spectra of  $\beta$ -peptide oligomers in various conformations and solvents, as well as computational interpretations of the experimental results, are currently under investigation in our laboratory.

## ■ ASSOCIATED CONTENT

### ■ Supporting Information

Experimental and simulated IR spectra of NEPA in D<sub>2</sub>O; simulated IR spectrum of peptide 1 in CDCl<sub>3</sub> and that of peptide 2 in CD<sub>3</sub>OD using different frequency map parameters; local-mode and eigen-mode frequency–frequency time-correlation functions and their biexponential fits;  $\beta$ -peptide structures used in our study in comparison with those from the literature;<sup>23,24</sup> dihedral angle distributions of three  $\beta$ -peptides; a comparison of experimental, simulated, and calculated IR spectra for the three  $\beta$ -peptides; vibrational couplings computed from the TDC scheme and wave function demixing scheme. This material is available free of charge via the Internet at <http://pubs.acs.org>.

## ■ AUTHOR INFORMATION

### Corresponding Author

\*Phone: (+86)-010-62656806. Fax: (+86)-010-62563167. E-mail: [jwang@iccas.ac.cn](mailto:jwang@iccas.ac.cn).

### Notes

The authors declare no competing financial interest.

## ■ ACKNOWLEDGMENTS

This work was supported by the National Nature Science Foundation of China (21173231, 20727001) and by the Chinese Academy of Sciences (Hundred Talent Fund).

## ■ REFERENCES

- (1) Gademann, K.; Ernst, M.; Hoyer, D.; Seebach, D. Synthesis and Biological Evaluation of a Cyclo- $\beta$ -Tetrapeptide as a Somatostatin Analogue. *Angew. Chem., Int. Ed.* **1999**, 38, 1223–1226.
- (2) Porter, E. A.; Wang, X.; Lee, H.; Weisblum, B.; Gellman, S. H. Antibiotics: Non-Haemolytic  $\beta$ -Amino-Acid Oligomers. *Nature* **2000**, 404, 565–565.
- (3) Imamura, Y.; Watanabe, N.; Umezawa, N.; Iwatsubo, T.; Kato, N.; Tomita, T.; Higuchi, T. Inhibition of  $\gamma$ -Secretase Activity by Helical  $\beta$ -Peptide Foldamers. *J. Am. Chem. Soc.* **2009**, 131, 7353–7359.
- (4) Karlsson, A. J.; Pomerantz, W. C.; Neilsen, K. J.; Gellman, S. H.; Palecek, S. P. Effect of Sequence and Structural Properties on 14-Helical  $\beta$ -Peptide Activity against *Candida albicans* Planktonic Cells and Biofilms. *ACS Chem. Biol.* **2009**, 4, 567–579.
- (5) Chung, Y.; Christianson, L. A.; Stanger, H. E.; Powell, D. R.; Gellman, S. H. A  $\beta$ -Peptide Reverse Turn that Promotes Hairpin Formation. *J. Am. Chem. Soc.* **1998**, 120, 10555–10556.
- (6) Chung, Y.; Huck, B. R.; Christianson, L. A.; Stanger, H. E.; Krauthausen, S.; Powell, D. R.; Gellman, S. H. Stereochemical Control of Hairpin Formation in  $\beta$ -Peptides Containing Dinipecotic Acid Reverse Turn Segments. *J. Am. Chem. Soc.* **2000**, 122, 3995–4004.
- (7) Daura, X.; Gademann, K.; Schafer, H.; Jaun, B.; Seebach, D.; van Gunsteren, W. F. The  $\beta$ -Peptide Hairpin in Solution: Conformational Study of a  $\beta$ -Hexapeptide in Methanol by NMR Spectroscopy and MD Simulation. *J. Am. Chem. Soc.* **2001**, 123, 2393–2404.

- (8) Langenhan, J. M.; Gellman, S. H. Effects of Alternative Side Chain Pairings and Reverse Turn Sequences on Antiparallel Sheet Structure in  $\beta$ -Peptide Hairpins. *Org. Lett.* **2004**, *6*, 937–940.
- (9) Doerksen, R. J.; Chen, B.; Yuan, J.; Winkler, J. D.; Klein, M. L. Novel Conformationally-Constrained  $\beta$ -Peptides Characterized by H-1 NMR Chemical Shifts. *Chem. Commun.* **2003**, 2534–2535.
- (10) Claridge, T. D. W.; Goodman, J. M.; Moreno, A.; Angus, D.; Barker, S. F.; Taillefumier, C.; Watterson, M. P.; Fleet, G. W. J. 10-Helical Conformations in Oxetane  $\beta$ -Amino Acid Hexamers. *Tetrahedron Lett.* **2001**, *42*, 4251–4255.
- (11) Hetenyi, A.; Mandity, I. M.; Martinek, T. A.; Toth, G. K.; Fulop, F. Chain-length-Dependent Helical Motifs and Self-Association of  $\beta$ -Peptides with Constrained Side Chains. *J. Am. Chem. Soc.* **2004**, *127*, 547–553.
- (12) Appella, D. H.; Christianson, L. A.; Klein, D. A.; Richards, M. R.; Powell, D. R.; Gellman, S. H. Synthesis and Structural Characterization of Helix-Forming  $\beta$ -Peptides: *trans*-2-Aminocyclopentanecarboxylic Acid Oligomers. *J. Am. Chem. Soc.* **1999**, *121*, 7574–7581.
- (13) Woll, M. G.; Fisk, J. D.; LePlae, P. R.; Gellman, S. H. Stereoselective Synthesis of 3-Substituted 2-Aminocyclopentanecarboxylic Acid Derivatives and Their incorporation into Short 12-Helical  $\beta$ -Peptides That Fold in Water. *J. Am. Chem. Soc.* **2002**, *124*, 12447–12452.
- (14) Park, J.; Lee, H.; Lai, J. R.; Kim, B.; Gellman, S. H. Accommodation of  $\alpha$ -Substituted Residues in the  $\beta$ -Peptide 12-Helix: Expanding the Range of Substitution Patterns Available to a Foldamer Scaffold. *J. Am. Chem. Soc.* **2003**, *125*, 8539–8545.
- (15) Peelen, T. J.; Chi, Y.; English, E. P.; Gellman, S. H. Synthesis of 4,4-Disubstituted 2-Aminocyclopentanecarboxylic Acid Derivatives and Their Incorporation into 12-Helical  $\beta$ -Peptides. *Org. Lett.* **2004**, *6*, 4411–4414.
- (16) Appella, D. H.; Christianson, L. A.; Karle, I. L.; Powell, D. R.; Gellman, S. H.  $\beta$ -Peptide Foldamers: Robust Helix Formation in a New Family of  $\beta$ -Amino Acid Oligomers. *J. Am. Chem. Soc.* **1996**, *118*, 13071–13072.
- (17) Raguse, T. L.; Lai, J. R.; Gellman, S. H. Environment-Independent 14-Helix Formation in Short  $\beta$ -Peptides: Striking a Balance between Shape Control and Functional Diversity. *J. Am. Chem. Soc.* **2003**, *125*, 5592–5593.
- (18) Guarracino, D. A.; Chiang, H. R.; Banks, T. N.; Lear, J. D.; Hodsdon, M. E.; Schepartz, A. Relationship between Salt-Bridge Identity and 14-Helix Stability of  $\beta^3$ -Peptides in Aqueous Buffer. *Org. Lett.* **2006**, *8*, 807–810.
- (19) Vaz, E.; Brunsveld, L. Stable Helical  $\beta^3$ -Peptides in Water via Covalent Bridging of Side Chains. *Org. Lett.* **2006**, *8*, 4199–4202.
- (20) Lee, M.; Raguse, T. L.; Schinnerl, M.; Pomerantz, W. C.; Wang, X.; Wipf, P.; Gellman, S. H. Origins of the High 14-Helix Propensity of Cyclohexyl-Rigidified Residues in  $\beta$ -Peptides. *Org. Lett.* **2007**, *9*, 1801–1804.
- (21) Vaz, E.; Pomerantz, W. C.; Geyer, M.; Gellman, S. H.; Brunsveld, L. Comparison of Design Strategies for Promotion of  $\beta$ -Peptide 14-Helix Stability in Water. *ChemBioChem* **2008**, *9*, 2254–2259.
- (22) Rueping, M.; Schreiber, J. V.; Lelais, G.; Jaun, B.; Seebach, D. Mixed  $\beta(2)/\beta(3)$ -Hexapeptides and  $\beta(2)/\beta(3)$ -Nonapeptides Folding to (P)-Helices with Alternating Twelve- and Ten-Membered Hydrogen-Bonded Rings. *Helv. Chim. Acta* **2002**, *85*, 2577–2593.
- (23) Hamm, P.; Woutersen, S.; Rueping, M. On the Thermal Stability of  $\beta$ -Peptides: A Two-Dimensional Vibrational Spectroscopy Study. *Helv. Chim. Acta* **2002**, *85*, 3883–3894.
- (24) Montalvo, G.; Waegle, M. M.; Shandler, S.; Gai, F.; DeGrado, W. F. Infrared Signature and Folding Dynamics of a Helical  $\beta$ -Peptide. *J. Am. Chem. Soc.* **2010**, *132*, 5616–5618.
- (25) Korendovych, I. V.; Shandler, S. J.; L. Montalvo, G.; DeGrado, W. F. Environment- and Sequence-Dependence of Helical Type in Membrane-Spanning Peptides Composed of  $\beta^3$ -Amino Acids. *Org. Lett.* **2012**, *14*, 3236–3236.
- (26) Baquero, E. E.; James, W. H.; Choi, S. H.; Gellman, S. H.; Zwier, T. S. Single-Conformation Ultraviolet and Infrared Spectroscopy of Model Synthetic Foldamers:  $\beta$ -Peptides Ac- $\beta^3$ -hPhe-NHMe and Ac- $\beta^3$ -hTyr-NHMe. *J. Am. Chem. Soc.* **2008**, *130*, 4784–4794.
- (27) Jackson, M.; Haris, P. I.; Chapman, D. Conformational Transitions in Poly(-lysine): Studies using Fourier Transform Infrared Spectroscopy. *Biochim. Biophys. Acta* **1989**, *998*, 75–79.
- (28) Krimm, S.; Bandekar, J. Vibrational Spectroscopy and Conformation of Peptides, Polypeptides, and Proteins. *Adv. Protein Chem.* **1986**, *38*, 181–364.
- (29) Torii, H.; Tasumi, M. Model Calculations on the Amide-I Infrared Bands of Globular Proteins. *J. Chem. Phys.* **1992**, *96*, 3379–3387.
- (30) Hamm, P.; Lim, M.; Hochstrasser, R. M. Structure of the Amide I Band of Peptides Measured by Femtosecond Nonlinear-Infrared Spectroscopy. *J. Phys. Chem. B* **1998**, *102*, 6123–6138.
- (31) Moran, A.; Mukamel, S. The Origin of Vibrational Mode Couplings in Various Secondary Structural Motifs of Polypeptides. *Proc. Natl. Acad. Sci. U.S.A.* **2003**, *101*, 506–510.
- (32) Wang, J.; Hochstrasser, R. M. Characteristics of the Two-Dimensional Infrared Spectroscopy of Helices from Approximate Simulations and Analytic Models. *Chem. Phys.* **2004**, *297*, 195–219.
- (33) Backus, E. H. G.; Bloem, R.; Donaldson, P. M.; Ihalaenen, J. A.; Pfister, R.; Paoli, B.; Caffisch, A.; Hamm, P. 2D-IR Study of a Photoswitchable Isotope-Labeled  $\alpha$ -Helix. *J. Phys. Chem. B* **2010**, *114*, 3735–3740.
- (34) Sengupta, N.; Maekawa, H.; Zhuang, W.; Toniolo, C.; Mukamel, S.; Tobias, D. J.; Ge, N.-H. Sensitivity of 2D IR Spectra to Peptide Helicity: A Concerted Experimental and Simulation Study of an Octapeptide. *J. Phys. Chem. B* **2009**, *113*, 12037–12049.
- (35) Maekawa, H.; Ge, N.-H. Comparative Study of Electrostatic Models for the Amide-I and -II Modes: Linear and Two-Dimensional Infrared Spectra. *J. Phys. Chem. B* **2010**, *114*, 1434–1446.
- (36) Paul, C.; Wang, J.; Wimley, W. C.; Hochstrasser, R. M.; Axelsen, P. H. Vibrational Coupling, Isotopic Editing, and  $\beta$ -Sheet Structure in a Membrane-Bound Polypeptide. *J. Am. Chem. Soc.* **2004**, *126*, 5843–5850.
- (37) Smith, A. W.; Tokmakoff, A. Amide I Two-Dimensional Infrared Spectroscopy of  $\beta$ -Hairpin Peptides. *J. Chem. Phys.* **2007**, *126*, 045109–045111.
- (38) Jones, K. C.; Peng, C. S.; Tokmakoff, A. Folding of a Heterogeneous  $\beta$ -Hairpin Peptide from Temperature-Jump 2D IR Spectroscopy. *Proc. Natl. Acad. Sci. U.S.A.* **2013**, *110*, 2828–2833.
- (39) Zhao, J.; Wang, J. Amide Vibrations and Their Conformational Dependences in  $\beta$ -Peptide. *J. Phys. Chem. B* **2010**, *114*, 16011–16019.
- (40) Baquero, E. E.; James, W. H.; Choi, S. H.; Gellman, S. H.; Zwier, T. S. Single-Conformation Ultraviolet and Infrared Spectroscopy of Model Synthetic Foldamers:  $\beta$ -Peptides Ac- $\beta^3$ -hPhe- $\beta^3$ -hAla-NHMe and Ac- $\beta^3$ -hAla- $\beta^3$ -hPhe-NHMe. *J. Am. Chem. Soc.* **2008**, *130*, 4795–4807.
- (41) James, W. H.; Baquero, E. E.; Shubert, V. A.; Choi, S. H.; Gellman, S. H.; Zwier, T. S. Single-Conformation and Diastereomer Specific Ultraviolet and Infrared Spectroscopy of Model Synthetic Foldamers:  $\alpha/\beta$ -Peptides. *J. Am. Chem. Soc.* **2009**, *131*, 6574–6590.
- (42) James, W. H.; Baquero, E. E.; Choi, S. H.; Gellman, S. H.; Zwier, T. S. Laser Spectroscopy of Conformationally Constrained  $\alpha/\beta$ -Peptides: Ac-ACPC-Phe-NHMe and Ac-Phe-ACPC-NHMe. *J. Phys. Chem. A* **2010**, *114*, 1581–1591.
- (43) Wang, J. Conformational Dependence of Anharmonic Vibrations in Peptides: Amide-I Modes in Model Dipeptide. *J. Phys. Chem. B* **2008**, *112*, 4790–4800.
- (44) Wang, J. Assessment of the Amide-I Local Modes in  $\gamma$ - and  $\beta$ -Turns of Peptides. *Phys. Chem. Chem. Phys.* **2009**, *11*, 5310–5322.
- (45) Ma, X.; Cai, K.; Wang, J. Dynamical Structures of Glycol and Ethanedithiol Examined by Infrared Spectroscopy, Ab Initio Computation, and Molecular Dynamics Simulations. *J. Phys. Chem. B* **2011**, *115*, 1175–1187.
- (46) Gnanakaran, S.; Hochstrasser, R. M. Conformational Preferences and Vibrational Frequency Distributions of Short Peptides in



Relation to Multidimensional Infrared Spectroscopy. *J. Am. Chem. Soc.* **2001**, *123*, 12886–12898.

(47) Bour, P.; Keiderling, T. A. Empirical Modeling of the Peptide Amide I Band IR Intensity in Water Solution. *J. Chem. Phys.* **2003**, *119*, 11253–11262.

(48) Ham, S.; Kim, J.-H.; Lee, H.; Cho, M. Correlation between Electronic and Molecular Structure Distortions and Vibrational Properties. II. Amide I Modes of NMA- $n\text{D}_2\text{O}$  Complexes. *J. Chem. Phys.* **2003**, *118*, 3491–3498.

(49) Schmidt, J. R.; Corcelli, S. A.; Skinner, J. L. Ultrafast Vibrational Spectroscopy of Water and Aqueous N-methylacetamide: Comparison of Different Electronic Structure/Molecular Dynamics Approaches. *J. Chem. Phys.* **2004**, *121*, 8887–8896.

(50) Hayashi, T.; la Cour Jansen, T.; Zhuang, W.; Mukamel, S. Collective Solvent Coordinates for the Infrared Spectrum of HOD in  $\text{D}_2\text{O}$  Based on an Ab Initio Electrostatic Map. *J. Phys. Chem. A* **2004**, *109*, 64–82.

(51) Jansen, T. I. C.; Knoester, J. A Transferable Electrostatic Map for Solvation Effects on Amide I Vibrations and its Application to Linear and Two-Dimensional Spectroscopy. *J. Chem. Phys.* **2006**, *124*, 044502–044511.

(52) Cai, K.; Han, C.; Wang, J. Molecular Mechanics Force Field-based Map for Peptide Amide-I Mode in Solution and its Application to Alanine Di- and Tripeptides. *Phys. Chem. Chem. Phys.* **2009**, *11*, 9149–9159.

(53) Reppert, M.; Tokmakoff, A. Electrostatic Frequency Shifts in Amide I Vibrational Spectra: Direct Parameterization Against Experiment. *J. Chem. Phys.* **2013**, *138*, 134116–134111.

(54) Hahn, S.; Ham, S.; Cho, M. Simulation Studies of Amide I IR Absorption and Two-Dimensional IR Spectra of  $\beta$  Hairpins in Liquid Water. *J. Phys. Chem. B* **2005**, *109*, 11789–11801.

(55) Wang, L.; Middleton, C. T.; Zanni, M. T.; Skinner, J. L. Development and Validation of Transferable Amide I Vibrational Frequency Maps for Peptides. *J. Phys. Chem. B* **2011**, *115*, 3713–3724.

(56) Scheurer, C.; Piryatinski, A.; Mukamel, S. Signatures of  $\beta$ -Peptide Unfolding in Two-Dimensional Vibrational Echo Spectroscopy: A Simulation Study. *J. Am. Chem. Soc.* **2001**, *123*, 3114–3124.

(57) Shi, J.; Zhao, J.; Yang, F.; Wang, J. Femtosecond Two-Dimensional Infrared Spectroscopy of N-Ethylpropionamide. *Acta Phys. Chim. Sin.* **2013**, *29*, 695–700.

(58) Seebach, D.; Overhand, M.; Kühnle, F. N. M.; Martinoni, B.; Oberer, L.; Hommel, U.; Widmer, H.  $\beta$ -Peptides: Synthesis by Arndt-Eistert Homologation with Concomitant Peptide Coupling. Structure Determination by NMR and CD Spectroscopy and by X-ray Crystallography. Helical Secondary Structure of a  $\beta$ -Hexapeptide in Solution and its Stability towards Pepsin. *Helv. Chim. Acta* **1996**, *79*, 913–941.

(59) Seebach, D.; L. Matthews, J.  $\beta$ -Peptides: A Surprise at Every Turn. *Chem. Commun.* **1997**, 2015–2022.

(60) Stewart, J. P. Optimization of Parameters for Semiempirical Methods V: Modification of NDDO Approximations and Application to 70 Elements. *J. Mol. Model.* **2007**, *13*, 1173–1213.

(61) Ma, X.; Wang, J. Differentiating Subtle Variation of Weak Intramolecular Hydrogen Bond in Vicinal Diols by Linear Infrared Spectroscopy. *J. Phys. Chem. A* **2009**, *113*, 6070–6076.

(62) Han, C.; Wang, J. Temperature-Dependence of the Amide-I Frequency Map for Peptides and Proteins. *Chin. J. Chem. Phys.* **2011**, *24*, 529–537.

(63) Phillips, J. C.; Braun, R.; Wang, W.; Gumbart, J.; Tajkhorshid, E.; Villa, E.; Chipot, C.; Skeel, R. D.; Kalé, L.; Schulten, K. Scalable Molecular Dynamics with NAMD. *J. Comput. Chem.* **2005**, *26*, 1781–1802.

(64) MacKerell, A. D.; Bashford, D.; Bellott, Dunbrack, R. L.; Evanseck, J. D.; Field, M. J.; Fischer, S.; Gao, J.; Guo, H.; Ha, S.; Joseph-McCarthy, D.; Kuchnir, L.; Kucera, K.; Lau, F. T. K.; Mattos, C.; Michnick, S.; Ngo, T.; Nguyen, D. T.; Prodhom, B.; Reiher, W. E.; Roux, B.; Schlenkrich, M.; Smith, J. C.; Stote, R.; Straub, J.; Watanabe, M.; Wiórkiewicz-Kucera, J.; Yin, D.; Karplus, M. All-Atom Empirical

Potential for Molecular Modeling and Dynamics Studies of Proteins<sup>†</sup>. *J. Phys. Chem. B* **1998**, *102*, 3586–3616.

(65) Zhu, X.; Koenig, P.; Hoffmann, M.; Yethiraj, A.; Cui, Q. Establishing Effective Simulation Protocols for  $\beta$ - and  $\alpha/\beta$ -Peptides. III. Molecular Mechanical Model for Acyclic  $\beta$ -Amino Acids. *J. Comput. Chem.* **2010**, *31*, 2063–2077.

(66) Jorgensen, W. L.; Chandrasekhar, J.; Madura, J. D.; Impey, R. W.; Klein, M. L. Comparison of Simple Potential Functions for Simulating Liquid Water. *J. Chem. Phys.* **1983**, *79*, 926–935.

(67) Wu, Y.; Wang, D. Theoretical Study on Side-Chain Control of the 14-Helix and the 10/12-Helix of  $\beta$ -Peptides. *J. Am. Chem. Soc.* **1999**, *121*, 9352–9362.

(68) Essmann, U.; Perera, L.; Berkowitz, M. L.; Darden, T.; Lee, H.; Pedersen, L. G. A Smooth Particle Mesh Ewald Method. *J. Chem. Phys.* **1995**, *103*, 8577–8593.

(69) Martyna, G. J.; Tobias, D. J.; Klein, M. L. Constant Pressure Molecular Dynamics Algorithms. *J. Chem. Phys.* **1994**, *101*, 4177–4189.

(70) Feller, S. E.; Zhang, Y.; Pastor, R. W.; Brooks, B. R. Constant Pressure Molecular Dynamics Simulation: The Langevin Piston Method. *J. Chem. Phys.* **1995**, *103*, 4613–4621.

(71) Wang, J.; Hochstrasser, R. M. Anharmonicity of Amide Modes. *J. Phys. Chem. B* **2006**, *110*, 3798–3807.

(72) Frisch, M. J.; Trucks, G. W.; Schlegel, H. B.; Scuseria, G. E.; Robb, M. A.; Cheeseman, J. R.; Scalmani, G.; Barone, V.; Mennucci, B.; Petersson, G. A.; Nakatsuji, H.; Caricato, M.; Li, X.; Hratchian, H. P.; Izmaylov, A. F.; Bloino, J.; Zheng, G.; Sonnenberg, J. L.; Hada, M.; Ehara, M.; Toyota, K.; Fukuda, R.; Hasegawa, J.; Ishida, M.; Nakajima, T.; Honda, Y.; Kitao, O.; Nakai, H.; Vreven, T.; Montgomery, J. A., Jr.; Peralta, J. E.; Ogliaro, F.; Bearpark, M.; Heyd, J. J.; Brothers, E.; Kudin, K. N.; Staroverov, V. N.; Kobayashi, R.; Normand, J.; Raghavachari, K.; Rendell, A.; Burant, J. C.; Iyengar, S. S.; Tomasi, J.; Cossi, M.; Rega, N.; Millam, J. M.; Klene, M.; Knox, J. E.; Cross, J. B.; Bakken, V.; Adamo, C.; Jaramillo, J.; Gomperts, R.; Stratmann, R. E.; Yazyev, O.; Austin, A. J.; Cammi, R.; Pomelli, C.; Ochterski, J. W.; Martin, R. L.; Morokuma, K.; Zakrzewski, V. G.; Voth, G. A.; Salvador, P.; Dannenberg, J. J.; Dapprich, S.; Daniels, A. D.; Farkas, O.; Foresman, J. B.; Ortiz, J. V.; Cioslowski, J.; Fox, D. J. *Gaussian 09*, revision A.02; Gaussian, Inc.: Pittsburgh, PA, 2009.

(73) Brooks, B. R.; Janežič, D.; Karplus, M. Harmonic Analysis of Large Systems. I. Methodology. *J. Comput. Chem.* **1995**, *16*, 1522–1542.

(74) Hamm, P.; Lim, M.; DeGrado, W. F.; Hochstrasser, R. M. The Two-Dimensional IR Nonlinear Spectroscopy of A Cyclic Penta-Peptide in Relation to Its Three-Dimensional Structure. *Proc. Natl. Acad. Sci. U.S.A.* **1999**, *96*, 2036–2041.

(75) Kubo, R. A Stochastic Theory of Line Shape. *Adv. Chem. Phys.* **1969**, *15*, 101–127.

(76) Oxtoby, D. W.; Levesque, D.; Weis, J. J. A Molecular Dynamics Simulation of Dephasing in Liquid Nitrogen. *J. Chem. Phys.* **1978**, *68*, 5528–5533.

(77) Mukamel, S. *Principles of Nonlinear Optical Spectroscopy*; Oxford University: New York, 1995.

(78) Kim, Y. S.; Hochstrasser, R. M. Dynamics of Amide-I Modes of the Alanine Dipeptide in  $\text{D}_2\text{O}$ . *J. Phys. Chem. B* **2005**, *109*, 6884–6891.

(79) Mukherjee, S.; Chowdhury, P.; Gai, F. Infrared Study of the Effect of Hydration on the Amide I Band and Aggregation Properties of Helical Peptides. *J. Phys. Chem. B* **2007**, *111*, 4596–4602.

(80) Seebach, D.; Abele, S.; Gademann, K.; Guichard, G.; Hintermann, T.; Jaun, B.; Matthews, J. L.; Schreiber, J. V.; Oberer, L.; Hommel, U.; Widmer, H.  $\beta^2$ - and  $\beta^3$ -Peptides with Proteinaceous Side Chains: Synthesis and Solution Structures of Constitutional Isomers, a Novel Helical Secondary Structure and the Influence of Solvation and Hydrophobic Interactions on Folding. *Helv. Chim. Acta* **1998**, *81*, 932–982.

(81) Wang, J.; Chen, J.; Hochstrasser, R. M. Local Structure of  $\beta$ -Hairpin Isotopomers by FTIR, 2D IR, and Ab Initio Theory. *J. Phys. Chem. B* **2006**, *110*, 7545–7555.

- (82) Roy, S.; Jansen, T. L. C.; Knoester, J. Structural Classification of the Amide I Sites of a  $\beta$ -Hairpin with Isotope Label 2DIR Spectroscopy. *Phys. Chem. Chem. Phys.* **2010**, *12*, 9347–9357.
- (83) Smith, A. W.; Lessing, J.; Ganim, Z.; Peng, C. S.; Tokmakoff, A.; Roy, S.; Jansen, T. L. C.; Knoester, J. Melting of a  $\beta$ -Hairpin Peptide Using Isotope-Edited 2D IR Spectroscopy and Simulations. *J. Phys. Chem. B* **2010**, *114*, 10913–10924.
- (84) Jansen, T. L. C.; Dijkstra, A. G.; Watson, T. M.; Hirst, J. D.; Knoester, J. Modeling the Amide I Bands of Small Peptides. *J. Chem. Phys.* **2006**, *125*, 044312–044319.
- (85) Hamm, P.; Woutersen, S. Coupling of the Amide I Modes of the Glycine Dipeptide. *Bull. Chem. Soc. Jpn.* **2002**, *75*, 985–988.
- (86) Dijkstra, A. G.; Jansen, T. L. C.; Knoester, J. Modeling the Vibrational Dynamics and Nonlinear Infrared Spectra of Coupled Amide I and II Modes in Peptides. *J. Phys. Chem. B* **2011**, *115*, 5392–5401.
- (87) Zhao, J.; Wang, J. Chain-length and Mode-Delocalization Dependent Amide-I Anharmonicity in Peptide Oligomers. *J. Chem. Phys.* **2012**, *136*, 214112–214111.